Silicon based microfluidic cell for terahertz frequencies

A. J. Baragwanath,[1] G. P. Swift,[1,2] D. Dai,[1] A. J. Gallant,[2] and J. M. Chamberlain[1]
[1]*Department of Physics, Durham University, South Road, Durham DH1 3LE, United Kingdom*
[2]*School of Engineering and Computing Sciences, Durham University, South Road, Durham DH1 3LE, United Kingdom*

(Received 29 January 2010; accepted 24 May 2010; published online 6 July 2010)

We present a detailed analysis of the design, fabrication and testing of a silicon based, microfluidic cell, for transmission terahertz time-domain spectroscopy. The sensitivity of the device is tested through a range of experiments involving primary alcohol/water mixtures. The dielectric properties of these solutions are subsequently extracted using a Nelder–Mead search algorithm, and are in good agreement with literature values obtained via alternative techniques. Quantities in the order of 2 μmol can be easily distinguished for primary alcohols in solution, even with the subwavelength optical path lengths used. A further display of the device sensitivity is shown through the analysis of commercial whiskeys, where there are clear, detectable differences between samples. Slight absorption variations were identified between samples of the same commercial brand, owing to a 2.5% difference in their alcoholic content. Results from data taken on subsequent days after system realignment are also presented, confirming the robustness of the technique, and the data extraction algorithm used. One final experiment, showing the possible use of this device to analyze aqueous biological samples is detailed; where biotin, a molecule known for its specific terahertz absorptions, is analyzed in solution. The device sensitivity is once again displayed, where quantities of 3 nmol can be clearly detected between samples. © *2010 American Institute of Physics*. [doi:10.1063/1.3456175]

I. INTRODUCTION

The use of terahertz (THz) radiation to analyze aqueous samples has long been hampered by strong water absorption. The permanent dipole of water dominates and often masks any specific THz absorption which may occur from a known molecule in solution. In addition, the high optical density of polar liquids throughout the THz regime means that with the low emitter powers currently available using conventional THz time domain spectroscopy (TDS), relatively thin samples ($>\sim 200$ μm) almost completely absorb the incident radiation. A direct solution to this problem has so far been circumvented by using reflection geometry (as opposed to transmission); however the reflection geometry optical arrangements are often difficult to align, the necessary mathematical analysis is complex, and the detected signals commonly weak. Given the wealth of THz properties predicted for many biological molecules, a more practical solution is desirable. To date, the analysis of biological samples at THz frequencies has mainly focused on dehydrated samples.[1] Given that proteins require water to function, a device enabling the analysis of such molecules in their natural environment would be invaluable.

Here, we present a possible solution to the "water problem" which currently hampers the analysis of polar liquids and aqueous biological samples at THz frequencies. The fabrication of a microfluidic cell constructed solely from silicon, a material inherently transparent to THz radiation, is presented. The cell is designed for use in a standard THz-TDS transmission system. The fundamental design characteristics of the cell focus on the importance of the knowledge of the optical path through a sample. The microfabrication techniques detailed in Sec. VI allow this path length to be defined to a high degree of accuracy, while the microfluidic design aspect keeps this path length to a minimum. The short optical path length allows for both sufficient sample interaction and strong signal detection. In this paper we demonstrate the sensitivity of the device through a range of THz-TDS experiments, including the analysis of primary alcohols, commercial whiskeys, and simple biological molecules in solution.

II. MICROFLUIDICS FOR THZ FREQUENCIES

The large optical density of water and other polar liquids at THz frequencies has resulted in the development of many novel devices which aim to minimise the THz path length through the sample. Previous work on hydrated proteins[2] utilized a brass cell with THz transparent quartz windows to contain samples. Here, a Teflon spacer was used to separate the brass plates by a distance of $\sim$250 μm. This device suffers from the fact that samples cannot be interchanged within quick succession and the optical path length cannot be determined to a high degree of accuracy. Other work on proteins[3] encapsulated samples in a polyethylene bag which was subsequently sandwiched between two methylpentene copolymer windows. This device is beneficial in that the distance between the two polymer windows can be altered, thus varying the optical path length. However, it suffers from many drawbacks including its cumbersome arrangement, multiple surface reflections, and the difficulties of interchanging samples.

To solve the problems relating to the interchanging of samples mentioned above, other groups have tried a more

conventional microfluidic approach. Standard materials for microfludic device fabrication such as polydimethylsiloxane (PDMS) suffer from vast THz absorption due to their high water content, making them unsuitable. Low THz-loss polymers such as Zeonor 1020R have been used to create suitable devices.[4] The use of plasma polymerised tetramethyldisiloxane is another possible emerging candidate for a polymer solution;[5] however, more detailed work still needs to be undertaken into the THz absorption properties of the material. Silicon-glass microfluidic devices have been demonstrated in the past,[6] though they are unsuitable for THz frequencies due to the scattering effects induced by the glass.

On first thoughts, silicon does not suggest itself as an obvious material for sole fabrication of microfluidic devices, due to its opaque nature at optical frequencies. The well known fact that silicon is inherently transparent to THz radiation has been exploited in previous work, in which silicon plates are used to contain the samples.[7] This device once again suffers from the fact that samples cannot be easily interchanged. Commercial products are available;[8] however the use of such products restricts the addition of any further functionality, such as the integration of plasmonic arrays,[9] antireflective structures,[10] mixing chambers, etc.

The transparent nature of the material, combined with the wealth of micromachining techniques available for silicon, makes it an ideal candidate to fabricate a THz microfluidic cell, with which samples can be easily changed.

III. DEVICE DESIGN

After selecting silicon as the fabrication material, our initial design was determined by two main features: The interaction chamber must have a well defined, controllable depth and samples must be able to be pumped through the device in turn. A simple design, incorporating input and output capillaries connected to a main chamber, was chosen. The capillaries were kept narrow (200 μm), to allow capillary action to draw fluid in and out of the chamber and help reduce pumping pressures. The chamber dimensions were kept large (1 cm^2) to allow for simple alignment in the THz measurement system. We estimated that a chamber depth in the region of 50 μm would provide a suitable optical path length to allow for sufficient sample interaction, while still allowing a strong THz signal to be detected, even with an optically dense sample. Previous reports provide calculations of the optimum thicknesses for a variety of samples to be analyzed using a transmission THz-TDS measurement: For water, a thickness of 130 μm at 0.5 THz is calculated, decreasing to 100 μm at 1.0 THz.[11] This indicates that thinner samples should be used as the frequency increases. With our broadband system, frequencies of up to 3 THz are achieved, thus justifying our 50 μm chamber depth.

IV. EXPERIMENTAL

All the experiments described in this paper used a standard THz-TDS transmission arrangement with a usable 3 THz bandwidth. The use of THz-TDS allows for the collection of both amplitude and phase information, allowing the optical properties of a material to be determined with relative ease. By taking a fast Fourier transform (FFT) of the time domain pulses, conventional spectroscopic data is revealed. For a comprehensive background on the principles of this technique, see Ref. 12. The optical arrangement used in these experiments utilized 600 mW, 20 fs pulses with 76 MHz repetition rate from a mode locked Ti:sapphire laser. THz radiation was generated using a GaAs photoconductive switch, after which the beam was passed through a series of 2″ off-axis parabolic mirrors to focus the radiation down to a point, at which the chamber of the microfluidic device was placed. Having interacted with the sample, the THz beam was subsequently focused onto a 500 μm ZnTe crystal, utilizing standard electro-optic detection techniques. All experiments were carried out in a nitrogen purged environment to reduce any absorption from water vapor in the atmosphere.

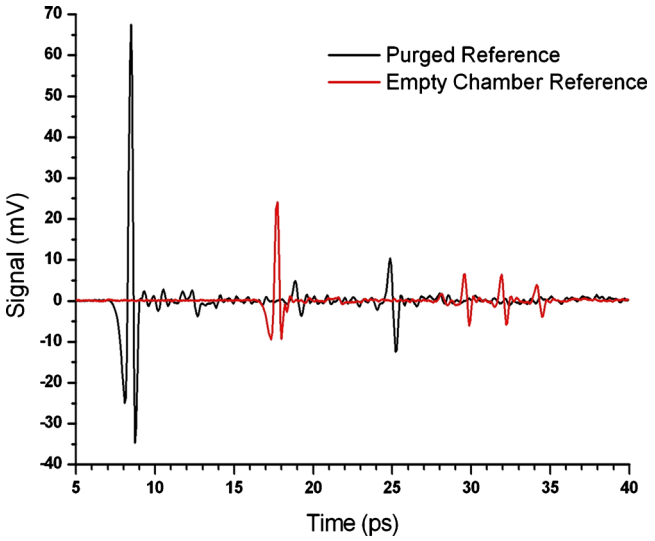

FIG. 1. (Color online) Comparison of the system reference with the empty chamber reference.

V. DEVICE FUNCTION AND ANALYSIS TECHNIQUES

The device function was initially investigated to see how the empty device behaved in the THz beam. By looking at Fig. 1, many features of the device function can be observed. First, the time delay of the main pulse compared to the free space reference is apparent. This time delay arises due to the high refractive index of silicon (3.42) at THz frequencies. It is this high refractive index which also causes the reduction in signal between the free space and the empty chamber measurements. The Fresnel equations predict a 30% reflection from each silicon–air interface. As four such boundaries are present in the device, only around 25% of the reference signal can expected to be detected after interaction with the chamber, as displayed by the relative pulse intensities in Fig. 1.

A system reflection in the reference scan can be seen occurring at 25 ps. With the introduction of the chamber, this reflection can be seen at 35 ps, and is preceded by reflections occurring from inside the silicon wafers at 30 ps and 32 ps, respectively.

Analysis was carried out using standard THz-TDS data extraction methods. As readings are taken in the time domain, samples with higher refractive indices delay the pulse more than a sample with a lower index. Crude estimations can be made of the refractive index of a sample by measuring the time delay of a sample pulse compared to a known reference pulse. A more refined approach was utilized for our experiments. Initially, a reference scan of the empty chamber was taken, $E_{\mathrm{ref}}(t)$, and, after filling the chamber with the sample, a further scan was taken, $E_{\mathrm{sam}}(t)$. By transforming the two pulses into the frequency domain (ν), the amplitude and phase of the measurements could be extracted. Then, by taking the ratio of the two spectra, $E_{\mathrm{sam}}(\nu)/E_{\mathrm{ref}}(\nu)$, the phase of the ratio, $\phi(\nu)$, was used to calculate the refractive index of the sample, $n_{\mathrm{sam}}(\nu)$ (Ref. 13)

$$n_{\mathrm{sam}}(\nu) = 1 + \frac{c}{2\pi\nu d}\phi(\nu). \tag{1}$$

Here, c is the speed of light and d is the thickness of the chamber. The value of the refractive index is critically dependant upon the thickness d, illustrating the fact that the thickness of a sample has to be known a high degree of accuracy to allow for accurate parameter determination.

The absorption coefficient $\alpha(\nu)$, was calculated using the amplitude of the ratio of the spectra, $A(\nu)$, through the following equation:

$$\alpha(\nu) = \frac{-2}{d}\ln\left\{A(\nu)\frac{[n_{\mathrm{sam}}(\nu)+n_{\mathrm{Si}}]^2}{n_{\mathrm{sam}}(\nu)(n_{\mathrm{Si}}+1)^2}\right\}, \tag{2}$$

where the real part of the refractive index of silicon is given by $n_{\mathrm{Si}}=3.42$. This value of $\alpha(\nu)$ can then be used to calculate the extinction coefficient $\kappa(\nu)$, and subsequently the real and imaginary parts of the complex dielectric function, $\varepsilon'(\nu)$ and $\varepsilon''(\nu)$, respectively.

The above equations do not take into account a possible Fabry–Perot effect which could occur in the chamber. Although such etalon effects were not apparent in the empty chamber reference pulses due to the high Fresnel losses (Fig. 1), for completeness, a third equation was derived, taking these effects into account[14]

$$\frac{E_{\mathrm{sam}}(\nu)}{E_{\mathrm{ref}}(\nu)} = \exp\left\{\frac{i2\pi\nu d}{c}[\tilde{n}_{\mathrm{sam}}(\nu)-1]\right\}\frac{\tilde{n}_{\mathrm{sam}}(\nu)(n_{\mathrm{Si}}+1)^2}{[\tilde{n}_{\mathrm{sam}}(\nu)+n_{\mathrm{Si}}]^2}\frac{1-\left(\frac{1-n_{\mathrm{Si}}}{n_{\mathrm{Si}}+1}\right)^2\exp\left(\frac{i4\pi\nu d}{c}\right)}{1-\left[\frac{\tilde{n}_{\mathrm{sam}}(\nu)-n_{\mathrm{Si}}}{\tilde{n}_{\mathrm{sam}}(\nu)+n_{\mathrm{Si}}}\right]^2\exp\left[\frac{i4\pi\nu d\tilde{n}_{\mathrm{sam}}(\nu)}{c}\right]}. \tag{3}$$

Here, $\tilde{n}_{\mathrm{sam}}(\nu)$ is the complex refractive index of the sample in the chamber where $\tilde{n}_{\mathrm{sam}}(\nu)=n_{\mathrm{sam}}(\nu)+i\kappa_{\mathrm{sam}}(\nu)$.

As we are dealing with a thin sample, the phase change at the silicon-sample boundaries is comparable to the phase change acquired through the sample, thus, an even more refined approach to that of Eqs. (1) and (2) must be used to extract the sample parameters. Such an approach takes the form of a Nelder–Mead search algorithm as detailed in Ref. 15. An error function incorporating both the experimental data and the theoretical Eq. (3) is defined, for which the algorithm finds the minimum value at each frequency. Using initial values for $n_{\mathrm{sam}}(\nu)$ and $\kappa_{\mathrm{sam}}(\nu)$ calculated using Eqs. (1) and (2), the algorithm finds the functions minimum point by varying these two parameters. Once the minimum is found, the final values of $n_{\mathrm{sam}}(\nu)$ and $\kappa_{\mathrm{sam}}(\nu)$ are returned.

A range of experiments was devised to assess the reproducibility, accuracy, and sensitivity of the device. These included the analysis of different primary alcohol/water mixtures, commercial whiskeys, and a simple biological molecule with known THz activity dissolved in solution. The results can be found in Sec. VII.

VI. DEVICE FABRICATION

Fabrication of the device was undertaken in a cleanroom environment. Initially, a 700 nm protective oxide layer was grown on a bare silicon wafer in a steam environment. Standard lithographic processes using S1813 photoresist were then used to define the capillaries and chamber on the polished side of the wafer [3700 rpm, 3 s exposure, 351 developer (351, H_2O: 1:3)]. The exposed oxide was etched using buffered hydrogen fluoride (HF) solution ($[NH_4]F$, HF: 4:1) leaving bare silicon regions. After removing the photoresist, the wafer was placed in 85 °C KOH until the chamber and capillaries had etched to the desired depth. A detailed surface profile of the chamber was acquired using a STIL surface profiler, returning the exact depth of the chamber. Typically, there is a surface roughness of the order of 1 μm over the whole 1 cm^2 area of the chamber.

After growing a further 700 nm protective oxide layer, a thicker photoresist AZ4562, was used to cover the reverse of the wafer. Circular input ports were defined using double-sided photolithographic alignment techniques which, once etched, would allow access to the previously etched capillaries [3700 rpm, 18 s exposure, 351 developer (3:1 H_2O)]. A reactive ion etch was used to remove the exposed oxide as opposed to the previously used buffered HF, to avoid resist delamination [Oxford Plasma Laboratory 80, 40 mTorr, 200 W, 32 SCCM (SCCM denotes cubic centimeter per minute at STP) CHF_3, 18 SCCM Ar, 30min, 10 °C Table Temp.). A XeF_2 etch was used to etch the ports through the wafer (Xactix e1, 175 cycles, 60 s cycle, 4 Torr XeF_2, 4 Torr N_2). After removal of the photoresist and remaining oxide layers, a device of the type shown in Fig. 2 was created.

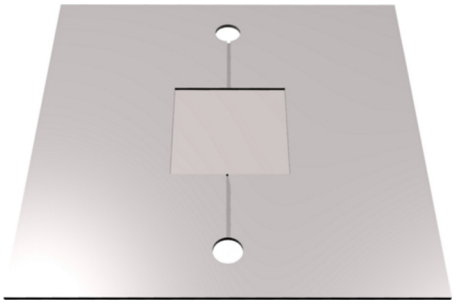

FIG. 2. (Color online) Diagram of capillaries, chamber, and ports etched into the silicon wafer.

To create the device solely out of silicon, the technique of silicon–silicon direct bonding was used to seal the chamber and capillaries.[16] This technique negates the need for an adhesive or polymer to bond the wafers. Such substances could not only have caused blockages to the capillaries but would have introduced unwanted reflections in the THz signal and may well have caused THz absorptions. The success of the bonding process relies critically upon the cleanliness, smoothness and hydrophilicity of the wafer surface. A stringent cleaning process was developed: 10 min piranha (H_2SO_4, H_2O_2, 1:1), de-ionised (DI) water rinse, 7 min UV exposure, isopropanol (IPA) rinse, DI rinse, 5 min piranha, DI rinse, 5 min HF etch (HF, H_2O, 1:10), DI rinse, 5 min piranha, DI rinse, spin dry. To increase the hydrophilicity of the silicon surface, we subjected the wafers to an oxygen plasma treatment (200 W, 100 SCCM O_2, 200 mtorr, 30 s), and followed with a 3 min hydration step in DI water. After spin drying, the wafers were brought into contact at one point to allow a bonding wave to initiate. After annealing the wafer pair at 500 °C for 4 h, the bonded system was analyzed using a thermal imaging camera to ensure that the bond was void-free and that the channels were fully sealed.

Now that a fully sealed silicon microfluidic device had been made, a reliable way of interchanging samples had to be devised. This was accomplished by fabricating PDMS coupling structures which would sit in the ports of the device, as depicted in Fig. 3b.

The coupling structures were fabricated by curing the

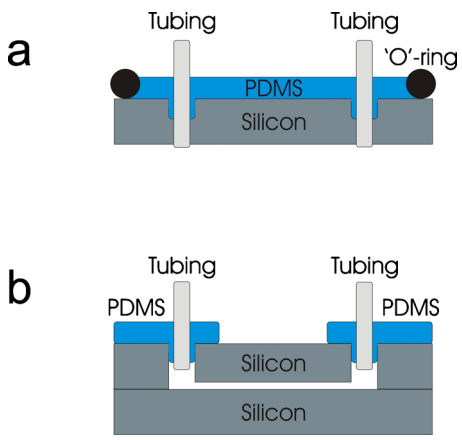

FIG. 3. (Color online) (a) Molding of the PDMS coupling structures on the dummy silicon wafer. (b) Schematic of how the PDMS coupling structures sit in the ports and allow access to the capillaries and chamber.

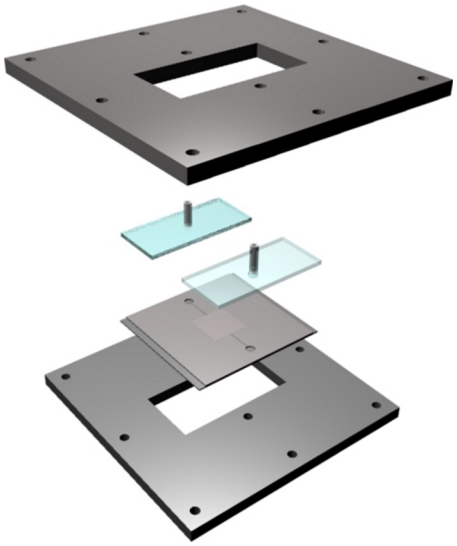

FIG. 4. (Color online) An exploded view of the system. Two metal plates are used to clamp the PDMS coupling structures in place. The central cut out in the metal plates allows the THz beam to pass solely through the chamber.

PDMS around 4 mm diameter tubing, on a dummy wafer [Fig. 3(a)]. The dummy wafer was fabricated using two subsequent etches of a silicon wafer. Two circular regions were defined using S1813 lithography, which matched the dimensions of the input ports on the device. These regions were etched to a depth of 300 μm using a XeF_2 etch. Patterning of the reverse of the wafer was done using AZ4562 photoresist. Double sided alignment was used to define 4 mm diameter circles in the resist, centered on the etched regions on the front side of the wafer. A further XeF_2 process then etched these regions through the remainder of the wafer. 4 mm diameter tubing was placed through the newly created holes and a rubber O-ring was glued to the wafer to contain the PDMS. Once poured over the device, the PDMS was cured at 120 °C for 20 min. The PDMS was subsequently peeled from the wafer, and rectangular sections were cut accordingly. After carefully aligning the coupling structures with the ports on the device, the whole system was placed in a clamping mechanism to apply even pressure between the PDMS and silicon to ensure that no leaks occur (Fig. 4).

The above device succeeds in several areas. Firstly, the device is fabricated from a THz transparent material–silicon. Secondly, the depth of the chamber is kept small so that strong signals can still be detected, even when using optically dense samples. Thirdly, the chamber depth cannot only be precisely controlled, but also measured, giving us a highly accurate determination of the optical path length of the THz beam. Fourthly, samples can be interchanged with ease by simply pumping fluids through the chamber by means of the PDMS coupling structures. This arrangement obviates the need to remove the device from THz beam; meaning no alignment discrepancies are incurred when interchanging samples. Finally, the design and construction method can be easily adapted to increase functionality through the integration of plasmonic structures or additional mixing chambers. These five advantages highlight the benefits of this device over previous solutions.

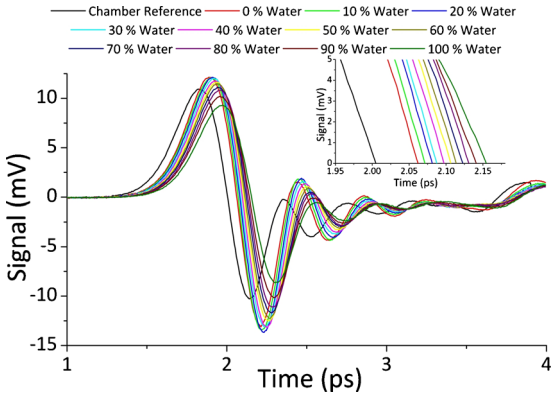

FIG. 5. (Color online) Time domain data for IPA/water mixture series.

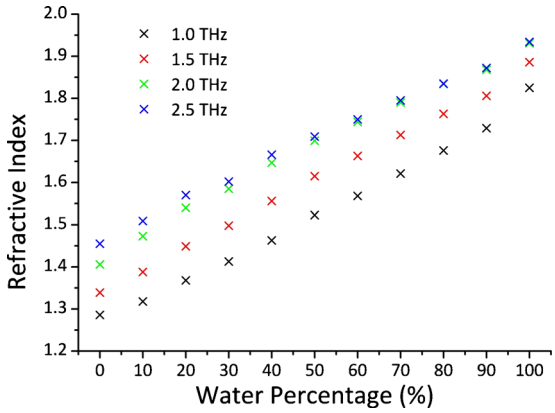

FIG. 7. (Color online) Analysis of the calculated refractive indices of different IPA/water mixtures, for selected frequencies.

VII. RESULTS

A. Primary alcohols

Initially, a simple experiment analyzing different IPA/water mixtures was undertaken. A range of mixtures was prepared, with the water content varying from 0% to 100% by volume, in 10% increments. The time domain results for this data can be seen in Fig. 5.

Examination of the intensity of the main pulse shows there is a clear decrease in the signal amplitude as the water concentration is increased, owing to the greater absorption of water over IPA. As the water concentration is increased, the pulse shifts further in time with respect to the chamber reference, resulting from the higher effective refractive index of the samples. An increase in intensity between the sample and the empty chamber reference is observed for the low water concentrations. This can be explained due to the improved refractive index matching between the sample and the silicon, as opposed to that of silicon and air. As the water concentration is increased, the increased absorption of the sample outweighs this improved matching. The refractive index of the solutions was extracted using the techniques detailed above (Fig. 6).

The results in Fig. 6 are in good agreement with data obtained via other techniques,[17] and clearly display the different optical properties of IPA and water at THz frequencies. The 3 mm focal spot of the THz beam, combined with an optical path length of 50 μm, means a volume of only 1.4 μl of liquid is analyzed in each scan. This highlights the sensitivity of the device: differences in the refractive index can be easily detected between 10% changes in alcohol concentration, even with the microliter quantities being analyzed, and the subwavelength sample interaction. In summary, the device can detect differences to the order of 2 μmol of IPA in solution. By analyzing these results at selected frequencies, a linear plot is produced (Fig. 7).

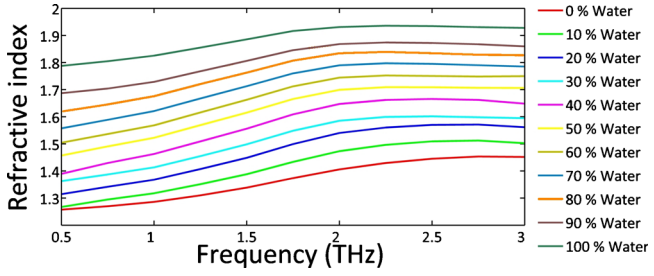

FIG. 6. (Color online) Calculated refractive indexes for IPA/water mixtures.

To the best of our knowledge, there is only one instance in the literature where the detailed analysis of IPA/water mixtures has been undertaken.[17] To allow for greater examination of our results, a further set of experiments was carried out using the same techniques, for an ethanol/water series. For a direct comparison to both work undertaken by reflection spectroscopy techniques[18–20] and transmission arrangements,[7] the real and imaginary parts of the complex dielectric function were plotted as a function of frequency (Fig. 8).

The results acquired for ethanol and water in Fig. 8 show the distinct differences between their complex dielectric function parameters in the THz regime. Furthermore, the results are comparable to those acquired in literature by reflection[18–20] and transmission arrangements[7] showing the validity of the device and the data extraction techniques.

The sensitivity to different alcohols was also displayed in a further experiment involving both ethanol and IPA. Samples of each alcohol were pumped, in turn, through the device. The results, displayed in Fig. 9, show the sensitivity and reproducibility of the device, with the distinct differences between the two samples being highlighted, while the two readings for each individual alcohol are almost indistinguishable from each other.

B. Commercial whiskeys

A further experiment was conducted into the analysis of different commercial whiskeys using this device. Figure 10 shows that clear differences can be detected between the samples. As all the samples had an alcohol content of 40% by volume, these differences can be attributed to the composition of the whiskeys (carbonyl compounds, carboxylic acids, and esters, for example), as distinct from their alcoholic content.

To assess the reproducibility and robustness of the device and the associated data extraction algorithms, a sample of "Famous Grouse" whiskey was tested on two subsequent

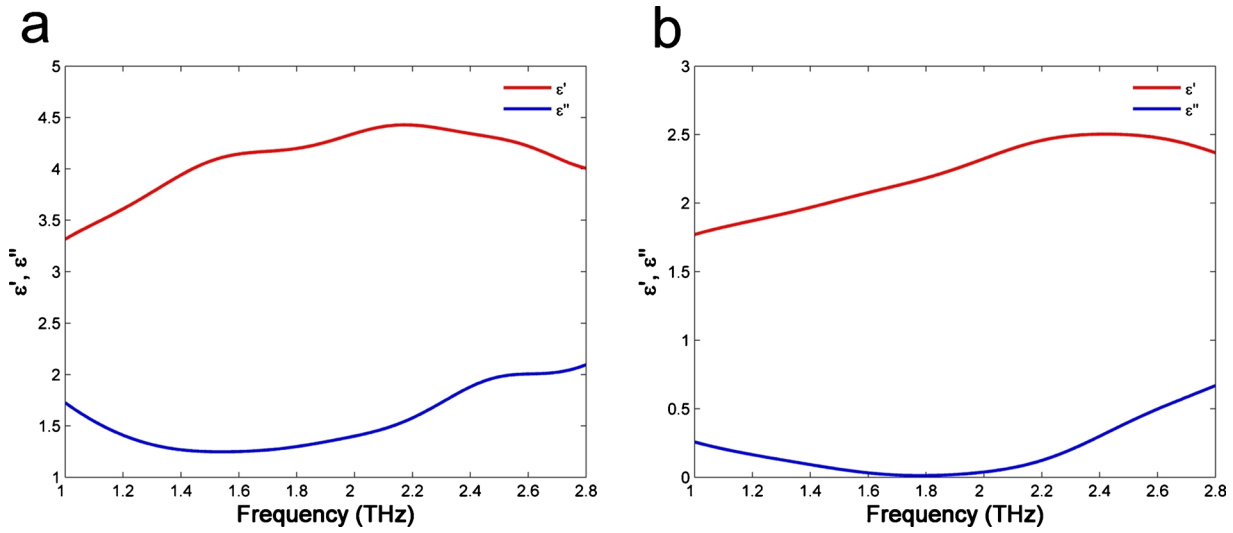

FIG. 8. (Color online) The real and imaginary parts of the complex relative dielectric constant for (a) water and (b) ethanol.

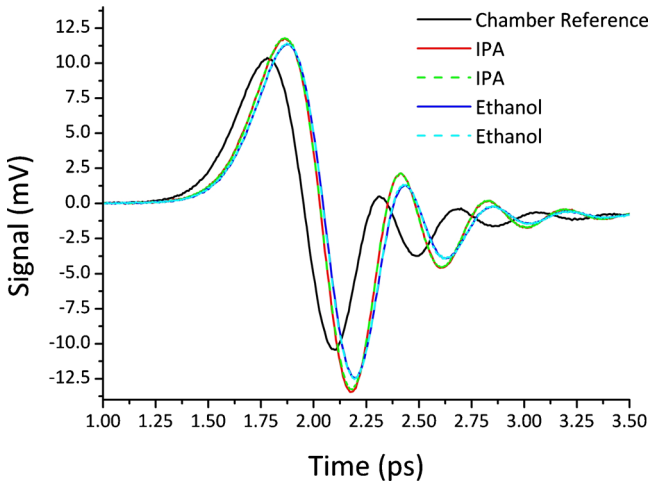

FIG. 9. (Color online) Time domain results for primary alcohols demonstrating the sensitivity and reproducibility of the device.

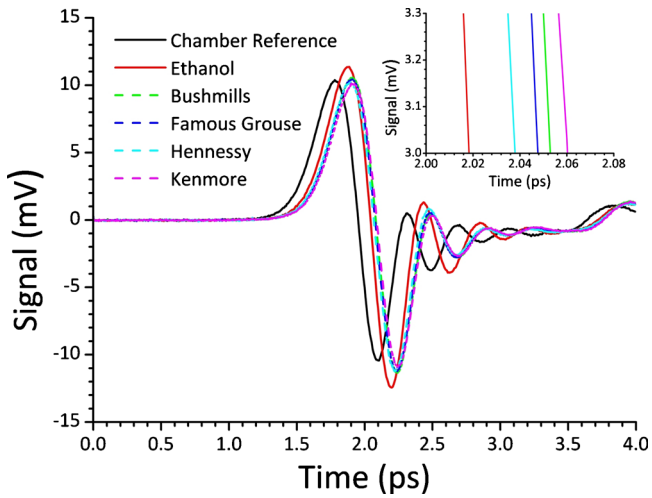

FIG. 10. (Color online) Time domain results for different commercial whiskeys.

days after a complete realignment of the device. The dielectric information was extracted for both sets of data, the results of which are displayed in Fig. 11.

The traces displayed in Fig. 11 have reduced chi-squared values of 2.43 and 2.19 for ε' and ε'', respectively, showing the data to be highly consistent, even after a complete realignment of the device, and the day to day variations expected with a THz-TDS arrangement. This confirms the reproducibility of the results obtained using the device, and the associated data extraction algorithms.

By taking alternative samples of the same whiskey ("Famous Grouse") with slightly different alcoholic content (37.5% and 40%, respectively), a further test of the device sensitivity was undertaken, the results of which are displayed in Fig. 12.

The results shown in Fig. 12 are consistent with the alcoholic content of the samples. The sample containing 40% alcohol has a lower ε'' value than the 37.5% sample. This result is to be expected, as the sample containing 40% alcohol will contain less water, which as demonstrated in Sec. VII A, is more absorbing than ethanol over the investigated frequency range. Reduced chi-squared results of 2.89 and 11.21 for ε' and ε'', respectively, are achieved when analyz-

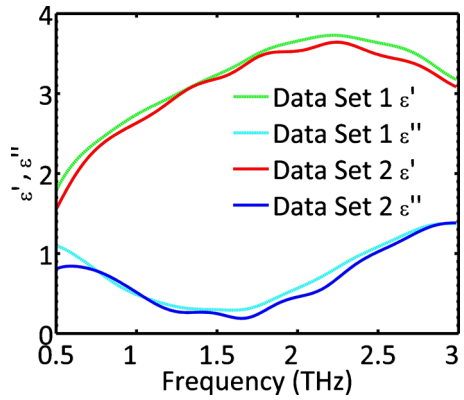

FIG. 11. (Color online) The dielectric constants extracted for the same whiskey sample, taken on subsequent days, after a complete realignment of the device.

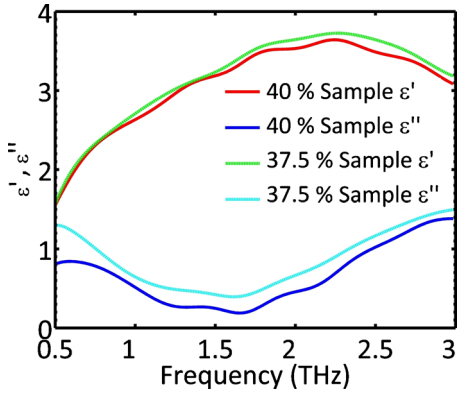

FIG. 12. (Color online) The dielectric constants extracted for different samples of the same brand of whiskey ("Famous Grouse"). The lower absorption exhibited by the 40% sample, is consistent with the composition of the two samples.

ing the two samples. These values are greater than the reduced chi-squared data calculated for the day to day variation in the spectroscopy arrangement. The results presented demonstrate how this device can be used to reliably distinguish between different commercial brands of whiskey, and also distinguish between the alcoholic content of the same whiskey blend.

C. Biotin solutions

Biotin has been well studied using THz radiation. Up until now, all analysis has been carried out using a dried or pellet form of the sample.[21] We mixed a powdered form of the molecule with de-ionised water to form a range of solutions covering a fully dissolved regime, to a heavily saturated solution. The transmission results can be seen in Fig. 13.

The decrease in signal intensity as the percentage of biotin in solution is increased can be clearly observed, owing to the strong absorption properties of this molecule in the THz regime. A slight decrease in time delay referenced to the empty chamber is also observed as the biotin percentage is increased. This can be accredited to the lower refractive index of the biotin compared to the water.

In comparison to previous work undertaken studying biotin samples prepared in a polyethylene matrix,[21] where frequency specific activity could be seen throughout the tested range, no such activity is observed here with the molecule in solution. The inset of Fig. 13 depicts the FFT of the data, where only blanket absorptions can be observed. The 0.5 g/l changes detected using the device, corresponds to a sensitivity of in the order of 3 nmol for biotin in solution. The demonstration of such sensitivity using microliter volumes at highly subwavelength thicknesses, confirms our original postulation concerning the initial design, and asserts this device as a possible means to analyze aqueous biological systems at THz frequencies.

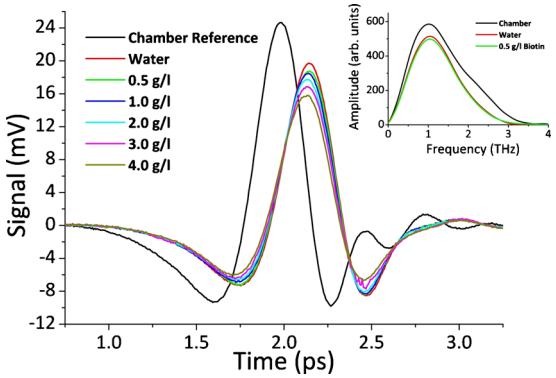

FIG. 13. (Color online) Time domain results for different aqueous solutions of biotin with FFT data (inset).

VIII. CONCLUSIONS

In this paper we have detailed the design, fabrication and testing of a silicon based, microfluidic device for transmission THz-TDS. Fabrication of the device employed standard lithographic and wafer bonding techniques, while PDMS coupling structures were fabricated to allow samples to be pumped through the device in turn. The device benefits from the fact that the optical path length is not only known to a high degree of accuracy, but it is kept small, such that strong signals can be detected even after interaction with optically dense samples.

After the analysis of the device function, a range of experiments involving alcohol/water mixtures were carried out, allowing for the extraction of optical constants. The data obtained was consistent with literature, showing the correct data extraction techniques were employed, and the system as a whole was reliable. Device sensitivity was displayed with 10% changes in alcohol/water concentrations being easily detectable, even with the 1.4 μl quantities being analyzed. These values show the device to be sensitive to the order of micromole quantities for primary alcohols in solution.

The sensitivity and reproducibility of the device was further displayed with more primary alcohol experiments, where it was used to reliably distinguish between IPA and ethanol. The analysis of commercial whiskeys showed the sensitivity of the device to molecules other than alcohols. Here, clear differences were observed between samples, owing to the composition of the sample as opposed to the alcoholic content alone. By analyzing the same whiskey sample on different days, after a realignment of the device, we proved our technique and data extraction algorithm to be robust, with only slight variations in the extracted data. The analysis of two samples of "Famous Grouse" whiskey, with a 2.5% difference in alcoholic content, show our device to be sensitive to the alcoholic content of the same whiskey blend, as well as being able to distinguish between commercial brands.

The analysis of a range of biotin solutions further highlighted the device sensitivity with quantities in the order of 3 nmol being distinguished. Such results demonstrate the feasibility for further analysis of aqueous biological systems at THz frequencies using this device.

[1]B. Yu, F. Zeng, Y. Yang, Q. Xing, A. Chechin, X. Xin, I. Zeylikovich, and R. R. Alfano, Biophys. J. **86**, 1649 (2004).
[2]J.-Y. Chen, J. R. Knab, S. Ye, Y. He, and A. G. Markelz, Appl. Phys. Lett. **90**, 243901 (2007).
[3]S. Ebbinghaus, S. J. Kim, M. Heyden, X. Yu, U. Heugen, M. Gruebele, D. M. Leitner, and M. Havenith, Proc. Natl. Acad. Sci. U.S.A. **103**, 12301

(2006).
[4]P. A. George, W. Hui, F. Rana, B. G. Hawkins, A. E. Smith, and B. J. Kirby, Opt. Express **16**, 1577 (2008).
[5]A. Abbas, P. Supiot, V. Mille, D. Guillochon, and B. Bocquet, J. Micromech. Microeng. **19**, 045022 (2009).
[6]N. Nguyen, C. Wang, T. N. Wong, L. N. Low, and S. S. Ho, International MEMS Conference, J. Phys.: Conf. Ser. **34**, 130 (2006).
[7]H. Kitahara, T. Yagi, K. Mano, M. W. Takeda, S. Kojima, and S. Nishizawa, J. Korean Phys. Soc. **46**, 82 (2005).
[8]www.specac.com
[9]Z. Tian, J. Han, X. Lu, J. Gu, Q. Xing, and W. Zhang, Chem. Phys. Lett. **475**, 132 (2009).
[10]Y. W. Chen, P. Y. Han, and X. C. Zhang, Appl. Phys. Lett. **94**, 041106 (2009).
[11]W. Withayachumnankul, B. M. Fischer, and D. Abbott, Opt. Express **16**, 7382 (2008).
[12]S. L. Dexheimer, *Terahertz Spectroscopy – Principles and Applications* (CRC, USA, 2007).
[13]P. U. Jepsen and B. M. Fischer, Opt. Lett. **30**, 29 (2005).
[14]A. G. Markelz, IEEE J. Sel. Top. Quantum Electron. **14**, 180 (2008).
[15]I. Pupeze, R. Wilk, and M. Koch, Opt. Express **15**, 4336 (2007).
[16]U. Gosele and Q. Y. Tong, Annu. Rev. Mater. Sci. **28**, 215 (1998).
[17]H. P. Merbold, Diploma thesis, University of Freiburg, 2006.
[18]P. U. Jepsen, U. Møller, and H. Merbold, Opt. Express **15**, 14717 (2007).
[19]P. U. Jepsen, J. K. Jensen, and U. Møller, Opt. Express **16**, 9318 (2008).
[20]U. Møller, D. G. Cooke, K. Tanaka, and P. U. Jepsen, J. Opt. Soc. Am. B **26**, A113 (2009).
[21]T. M. Korter and D. F. Plusquellic, Chem. Phys. Lett. **385**, 45 (2004).